Published in final edited form as:
Dev Biol. 2008 May 15; 317(2): 585–599. doi:10.1016/j.ydbio.2008.03.007.

Septate Junctions are Required for Ommatidial Integrity and Blood-Eye Barrier Function in *Drosophila*

Swati Banerjee[1], **Roland J. Bainton**[2], **Nasima Mayer**[2], **Robert Beckstead**[3], and **Manzoor A. Bhat**[1,4,5,6,*]

1 *Department of Cell and Molecular Physiology, University of North Carolina School of Medicine, Chapel Hill, NC 27599*

4 *Curriculum in Neurobiology, University of North Carolina School of Medicine, Chapel Hill, NC 27599*

5 *UNC-Neuroscience Center, University of North Carolina School of Medicine, Chapel Hill, NC 27599*

6 *Neurodevelopmental Disorders Research Center, University of North Carolina School of Medicine, Chapel Hill, NC 27599*

2 *Department of Anesthesia, University of California, San Francisco San Francisco, California 94143*

3 *Howard Hughes Medical Institute, University of Utah, Salt lake City, UT 84112*

Abstract

The anatomical organization of the *Drosophila* ommatidia is achieved by specification and contextual placement of photoreceptors, cone and pigment cells. The photoreceptors must be sealed from high ionic concentrations of the hemolymph by a barrier to allow phototransduction. In vertebrates, a blood-retinal barrier (BRB) is established by tight junctions (TJs) present in the retinal pigment epithelium and endothelial membrane of the retinal vessels. In *Drosophila* ommatidia, the junctional organization and barrier formation is poorly understood. Here we report that septate junctions (SJs), the vertebrate analogs of TJs, are present in the adult ommatidia and are formed between and among the cone and pigment cells. We show that the localization of Neurexin IV (Nrx IV), a SJ-specific protein, coincides with the location of SJs in the cone and pigment cells. Somatic mosaic analysis of *nrx IV* null mutants shows that loss of Nrx IV leads to defects in ommatidial morphology and integrity. *nrx IV* hypomorphic allelic combinations generated viable adults with defective SJs and displayed a compromised blood-eye barrier (BEB) function. These findings establish that SJs are essential for ommatidial integrity and in creating a BEB around the ion and light sensitive photoreceptors. Our studies may provide clues towards understanding the vertebrate BEB formation and function.

Keywords

Ommatidium; photoreceptors; cone cells; pigment cells; Neurexin IV

*Corresponding author: Manzoor Bhat, Neuroscience Research Building, NRB #5109, 103 Mason Farm Road, University of North Carolina School of Medicine, Chapel Hill, NC 27599-7545, Tel: 919-966-1018, Fax: 919-843-2777, Email: Manzoor_Bhat@med.unc.edu.

Introduction

The *Drosophila* compound eye is composed of about eight hundred units, the ommatidia, which are arranged in a hexagonal array to produce a stereotyped pattern. Each ommatidium consists of eight photoreceptors (PRs), four cone cells (CCs) and three types of pigment cells (PCs) (Tomlinson and Ready, 1987; Cagan and Ready, 1989; Wolff and Ready, 1991a; reviewed in Wolff and Ready, 1993). The eye develops from a single layer of proliferative epithelial cells, the eye imaginal disc, which is initially unpatterned during the first and second larval instar stages. Differentiation begins from the mid-third instar and is controlled by genes such as *eyeless*, *dachshund*, *sine oculis* and *eyes absent* (Chen et al., 1997; Halder et al., 1998; Mardon et al., 1994; Wolff, 2003). An indentation of the epithelium, called the morphogenetic furrow, forms in the third-instar eye imaginal disc. Anterior to the furrow, the cells divide asynchronously while posterior to the furrow, the cells begin to arrange into evenly spaced ommatidial precursor clusters and first differentiate into PR neurons (Tomlinson and Ready, 1987; Cagan and Ready, 1989; Wolff and Ready, 1991a). The non-neuronal CCs are added to each ommatidial cluster after the specification of the PRs in the late third instar eye disc (Tomlinson, 1988). The PCs and the sensory units (bristles) are recruited during the pupal stage, thereby completing the ommatidial assembly (Cagan and Ready, 1989; Wolff and Ready, 1993). Recent studies on the phenotypic characterization of *sparkling*, *bar*, and *cut* mutants have revealed important aspects of CC and/or PC functions during eye development (Blochlinger et al., 1993; Fu and Noll, 1997; Hayashi et al., 1998; Higashijima et al., 1992). However, CCs and PCs have received much less attention compared to the more extensively studied PRs, thus leading to gaps in our understanding of their range of functions.

The eye serves as a visual transduction machinery to perform photoreception and transduction functions in both vertebrates and invertebrates. In vertebrates, the retina contains two types of specialized PRs: rods and cones. The rods are more numerous than cones but both contain stacks of membranous discs which primarily perform the photoreception and phototransduction (Smith, 2002). The vertebrate retinal pigment epithelium forms an outer blood-retinal barrier (BRB) by separating the neural retina from the fenestrated capillaries in the choroids. This barrier depends upon TJs within the apical junctional complexes that bind neighboring cells (Williams and Rizzolo, 1997). Recent studies on the BRB in vertebrate models and human have highlighted its importance in many human ocular disorders, such as macular edema, diabetic retinopathy and retinitis pigmentosa (Vinores et al., 1999). One of the major causes of a BRB dysfunction in vertebrates is an increased permeability and/or structural alterations of the occluding TJs (Peng et al., 2003).

The PRs that form the core of the *Drosophila* ommatidium are housed within specially designed subcellular compartments that serve to maximize the amount of light absorbing membranes and molecules (Hardie and Raghu, 2001; Kumar and Ready, 1995). The PRs have densely packed microvilli forming the cylindrical rhabdomeres that form the seat of the phototransduction cassette as the rhabdomere membrane contains large quantities of light sensitive opsin and channel proteins (Hardie and Raghu, 2001; Ranganathan et al., 1995). For phototransduction to occur, these channel proteins and the PR units need to be protected from the circulating hemolymph, thereby raising a strong possibility of the existence of a protective blood-eye barrier (BEB) in the *Drosophila* retina. A detailed description of various forms of cell-cell junctions in *Drosophila* embryos (Tepass and Hartenstein, 1994), *Musca domestica* (reviewed in Carlson et al., 2000) and other insects (Lane, 2001) provided insights into the various forms of junctions in insects and their putative functions. Although TJs in *Drosophila* embryos and larvae have never been observed (Tepass and Hartenstein, 1994; Carlson et al., 2000; Tepass et al., 2001), fly homologs of vertebrate TJ proteins, Claudins, are present in *Drosophila* and localize to septate junctions (SJs) in embryonic epithelia cells (Behr et al., 2003; Wu et al., 2004) and glial cells (Banerjee and Bhat, unpublished data). SJs are a

specialized form of cell-cell junctions that display a characteristic electron-dense ladder-like structure, hence the name septate junctions, and have been shown to perform a barrier function in epithelia and glial cells (Auld et al., 1995; Banerjee and Bhat, 2007; Banerjee et al., 2006; Baumgartner et al., 1996; Faivre-Sarrailh et al., 2004). However, the presence of SJs in the adult *Drosophila* ommatidia or the cell types that might establish these junctions are still unknown.

Here, we report that SJs are present in the adult *Drosophila* ommatidia between and among the CCs and PCs. Immunofluorescence localization of a SJ-specific marker, Neurexin IV (Nrx IV) correlates with the ultrastructural presence of SJs in the developing and adult ommatidia. Using somatic clonal analysis, we demonstrate that Nrx IV function is essential for the maintenance of the ommatidial integrity in the developing and adult *Drosophila* eye. In addition, we show that viable hypomorphic *nrx IV* mutant combinations have altered distribution of Nrx IV in the adult CCs and PCs and a compromised BEB function.

Materials and Methods

Drosophila Stocks

Canton S strain was used as wild type. All *nrx IV* alleles used in this study have been previously reported in Baumgartner et al. (1996). All other fly reagents used in this study were obtained from the Bloomington Stock Center, Indiana.

Histology, Scanning electron microscopy (SEM) and Transmission electron microscopy (TEM)

Histology, fixation, sectioning, and SEM of adult eyes were carried according to published procedures with minor modifications (Cagan and Ready, 1989; Longley and Ready, 1995). Briefly adult eyes or pupal or larval discs were fixed in 2% glutaraldehyde in 0.1M sodium cacodylate buffer, pH 7.2, for 3 hours at room temperature followed by three 5 min washes in 0.1M sodium cacodylate buffer, pH 7.2. The tissues was postfixed in 1% osmium tetroxide in 0.1M sodium cacodylate buffer, pH 7.2 for one hour followed by three 5 min washes in deionized water. The tissues were then dehydrated in 30, 50, 75, and 95% ethanol for 10 min each followed by two 10 min steps in absolute ethanol and propylene oxide. The tissue was then infiltrated with 1:1 propylene oxide and Spurr's resin in propylene oxide for 3 hours followed by overnight infiltration in 100% Spurr's resin. The tissue was embedded in flat molds in 100% Spurr's resin for 24 hrs at 70°C. For initial light microscopic analysis and depth of the tissues, 1μm thick sections were cut with a glass knife, mounted on a glass slide and stained with 1% toluidine blue in 1% sodium borate for 30 seconds at 60 C. Once the desired area of the tissues was identified 60–70nm ultrathin sections were cut with a diamond knife and mounted on a 200 or 300 mesh copper grids, and double stained with 4% aqueous uranyl acetate for 15 minutes, followed by Reynolds' lead citrate for 7 minutes. The grids were washed in deionized water and allowed to dry at room temperature and analyzed on LEO EM 910 transmission electron microscope equipped with a high-resolution digital camera. All images were then processed with Adobe Photoshop Software.

Immunohistochemistry

Immunostaining of imaginal discs, pupal and adult eyes was done as previously described (Izaddoost et al., 2002). Primary antibodies used for immunofluorescence staining were: rabbit anti-Nrx IV (Baumgartner et al., 1996); guinea pig anti-Dlg (P. Bryant, UC, Irvine), rat anti-Crumbs (Bhat et al., 1999); mouse anti-Cadherin (Oda et al., 1994); mouse anti-Elav (DSHB, Iowa) and mouse anti-chaoptin (DSHB, Iowa). All secondary antibodies used in this study were from Jackson Immunochemicals. Images were captured on a BioRad Radiance 2000 confocal microscope and processed with Adobe PhotoShop software.

Somatic mosaic analysis in *nrx IV* mutants

Clones of cells lacking *nrx IV* were generated by *FLP*-mediated mitotic recombination with two *nrx IV* null alleles by subjecting *yw, hsp70-flp/+; nrx IV^{4304},FRT80B/w^{+}FRT80B* or *yw, hsp70-flp/+; nrx IV^{4025},FRT80B/w^{+}FRT80B* larvae 24–48 hours after egg lay to a single heat shock at 38.5°C in a water bath for 1 hour and 30 minutes (Xu and Rubin, 1993). For adult eye clonal analysis, clones were visually identified and the eyes were processed for SEM or TEM as described above. For TEM analysis at least 3 large and 5 small independent clones were processed from adults of two *nrx IV* null alleles (*nrx IV^{4304}* and *nrx IV^{4025}*) (Baumgartner et al., 1996). For light microscopic phenotypic evaluation, at least 5 independent eyes with large mutant clones (covering a space of more than 10 ommatidia) from *nrx IV* null alleles (*nrx IV^{4304}* and *nrx IV^{4025}*) were analyzed. Depending upon the area and the extent of the *nrx IV* mutant clone size, we performed either longitudinal or cross sectional analysis. Cross section clones were analyzed within a depth anywhere between 15–30μm at 70nm thickness and longitudinal clones were analyzed within a depth of 10 μm at 70nm thickness.

Sequence Analysis of *nrx IV* Alleles

For sequencing of the genomic DNA by PCR, manufacturer's instructions were followed and wherever necessary standard molecular biology protocols were used. Overlapping M13forward- and M13reverse-extended primers which spanned the entire genomic region of *Drosophila NRX IV* were as follows: F102-TGTAAA ACGACGGCCAGTGGAGTGTAAAGTGCACTCC, F460-TGTAAAACGACGGCC AGTCGTCCTCACGGCCACATCATC, R708-CAGGAAACAGCTATGACCTAGAGTT GCCATCGGAGTTG, F837-TGTAAAACGACGGCCAGTCTCTACGGTTGCGAT TAC, R1337-CAGGAAACAGCTATGACCGAAGAGATATCCCTCTCC, F1224-TGTA AAACGACGGCCAGTGGGCGCTGTATCTAGGTGGTG, R2109-CAGGAAACAGCT ATGACCGGTCACTGGGAAAGGTTCTAG, F2015-TGTAAAACGACGGCCAGTGG AGCTGTTTGCCATACA, R2495-CAGGAAACAGCTATGACCTCCAGACTGTTCG AATCG, F2852-TGTAAAACGACGGCCAGTTCCGTCCCTTCTCTTGGTGGA, R3221 CAGGAAACAGCTATGACCACGGCAATCGCAGCTGTAGCC, F3108-TGTAAAACG ACGGCCAGTGCACTGCTGCTGAACGGAAAG, R3815-CAGGAAACAGCTATGAC CTGGCTCCACTCCGCAGAAATC, F3656-TGTAAAACGACGGCCAGTCTCAGC GGATGCTCAATTC, and R4171-CAGGAAACAGCTATGACCTCGCTGTTGCGTG TCTAAG.

Adult Fly Dye Injection Assay Confocal Images of Dissected Fly Brains and Quantitation of Dye Leakage

Adult flies were hemolymph injected with 100nl of 50mg/ml 3kDa FITC-Dextran dye (Molecular Probes). Retinal fluorescent images were acquired after overnight recovery as described in Bainton et al. (2005). Briefly, after injection flies were allowed to recover overnight and anesthetized with CO_2 and placed in cold phosphate buffered saline (PBS, pH 7.2). The heads were removed manually with forceps and proboscis removed by pulling outwards and quickly placed in 3.7% paraformaldehyde and incubated for 15 minutes at room temperature. Brains were then dissected from the cuticle leaving the retina intact in cold PBS and transferred to 0.5ml PBS and then to mounting media (DakoCytomation Fluorescent Mounting medium) for 10 minutes. Brains were mounted retinal side down on glass slides, covered with media and a coverslip and sealed with clear nail polish. At this stage brains were either immediately processed for confocal analysis or stored at −20°C for up to a week before confocal analysis. Confocal images were acquired on a Zeiss LSM510 confocal microscope and images were taken at 16–21μm depth from the brain surface with a 40X H_2O objective. Laser and detector gains were established based on wild type animal's internal brain auto-fluorescence. A square of 1656 pixels was drawn on different parts of the wild type brain

parenchyma image and gains were set to maintain a fluorescence intensity of 3–7 units per 1656 pixels on the wild type animals. Images of *nrx IV* hypomorph brains were taken at the same confocal settings, depth of section and anatomic location. Pixel intensities for squares of 1656 pixels were take in different parts of the mutant brains to establish a range of fluorescence intensity for each hypomorphic combination. Fluorescent dye penetration was ranked by range of pixel intensity for each allelic combination. Using this method relative humoral barrier leakiness was established and ranked.

Results

Spatiotemporal Localization of SJs During Ommatidial Development

The *Drosophila* ommatidium is a stereotyped assembly of elongated sensory neurons, the PRs, which are in close proximity to the accessory CCs and PCs (Tomlinson and Ready, 1987; Cagan and Ready, 1989; Longley and Ready, 1995). Many studies have been carried out that addressed the cellular aspects of ommatidial differentiation and development, however, the junctional organization between various cell types in the ommatidia remain less understood. We sought to investigate the spatiotemporal localization of SJs in the developing and adult eye. As shown in Fig. 1A, a longitudinal section through the eye disc of third-instar larva shows the presence of goblet-shaped retinal epithelial cells that are in the process of differentiation. A low magnification toluidine blue stained section of the disc showed that the morphogenetic furrow is about 5 differentiating ommatidial units away from the posterior edge (data not shown). At this stage the eye disc is surrounded by the peripodial membrane and the apical surface of the retinal epithelial cells is highly enriched with the microvilli that face the peripodial cavity (ppc, Fig. 1A). The peripodial cavity contains extracellular fluid that separates the peripodial membrane and the retinal epithelial cells (Carlson et al., 1998). A higher magnification of a region from Fig. 1A (arrowhead) is shown in Fig. 1B. The boxed region (Fig. 1B) at a higher magnification shows the apical microvilli (black arrowheads, Fig. 1C), and adherens junctions (AJs) (white arrow, Fig. 1C). Basal to the AJs are short stretches of ladder-like pleated SJs (black arrows, Fig. 1C). Similarly, longitudinal section of the wild type early pupal eye disc reveals the presence of microvilli at the apical surface of the retinal epithelium (black arrowheads, Fig. 1D, E), AJs (white arrows, Fig. 1D, E) and stretches of pleated SJs (black arrows, Fig. 1D, E). These data indicate that the differentiating retinal epithelial cells at these stages possess SJs.

As the developing eye disc differentiates into an adult ommatidium, the retinal epithelial cells stretch along their longitudinal axis and attain different cell fates. To determine which cell types contain the SJs we carried out the ultrastructural analysis of the adult eye. A cross-section through the adult ommatidia at low magnification shows the arrangement of the CCs surrounded by the PCs (Fig. 1F). At a higher magnification, a cluster of four CCs of a single ommatidium below the level of the lens and the pseudocone show the presence of extensive stretches of SJs (arrowheads, Fig. 1G) between the CC cell membranes. At this level the CCs are situated above the PRs. At a higher magnification, the SJs between the CCs (arrowheads, Fig. 1H) are clearly visualized as pleated ladder-like structures. The SJs are also present between the PCs (arrowheads, Fig. I) as well as between the CC and PCs (Fig. 1I, black arrowheads). These ultrastructural data demonstrate the presence of SJs between the CCs and the PCs in the adult *Drosophila* ommatidium.

Lens Secreting Cone and Pigment Cells Form SJs

Pioneering work by Don Ready and colleagues (Tomlinson and Ready, 1987; Cagan and Ready, 1989; also reviewed in Wolff and Ready, 1993) provided an anatomical picture with a precise placement of the various cell types that orchestrate the organization of a *Drosophila* ommatidium (Fig. 2A). The details of the intercellular interactions and the formation of

junctions, especially the SJs, have remained unclear. In order to gain a better insight into the location of SJs along the length of the adult ommatidium, we carried out TEM analysis of longitudinal sections of the eye. A longitudinal section of the apical half of the ommatidium at a lower magnification (Fig. 2B) resembles the schematic shown in Fig. 2A. The adult ommatidium is a precise assembly of PRs and accessory cells (Fig. 2B). The apical most area is the corneal lens (L, Fig. 2B) below which is the pseudocone cavity (psc). There are primary PCs that form the walls of the pseudocone chamber and four CCs that act as both the floor of the pseudocone and roof of the underlying rhabdomeres of the photoreceptors (rb, Fig. 2B). At a higher magnification, the longitudinal section through an ommatidium (Fig. 2C) shows the presence of extensive SJs that run along the length of the CC membranes (black arrowheads, Fig. 2C) located basally to the AJs (white arrowheads, Fig. 2C, D). At an even higher magnification, the surface of the CCs facing the pseudocone is covered with small microvilli (black arrows, Fig. 2D) which aid in the secretion of the lens material. The CC membranes display extensive stretches of SJs (black arrowheads, Fig. 2D, E), and occasionally form loops with long stretches of SJs (black arrowheads, Fig. 2E). These data demonstrate the presence of SJs in the apical region of the CCs as observed in other embryonic epithelial cells (Faivre-Sarrailh et al., 2004).

As depicted in the longitudinal schematic of the ommatidium (Fig. 2A), the basal region or the floor of the adult ommatidium contains the CC feet and stress-fiber filled, flattened endfeet of the secondary and tertiary pigment cells. These endfeet display a fenestrated appearance. A longitudinal section through the bottom of the retina shows the fenestrated membrane (FM, Fig. 2F, G). Also note the cavity where photoreceptor rhabdomeres are located (Fig. 2F, RC). The axons of the photoreceptors (Ax) pass in between the CC endfeet and the pigment cell feet (Fig. 2F). At a higher magnification the pigment cell end feet show extensive fenestrations (Fig. 2G). Next we analyzed the presence of SJs in the basal region around the CC feet and the fenestrated membrane (Fig. 2H). Thin cone cell processes starting from the apical region near the pseudocone reach to the bottom of the ommatidium and form bulb shaped end feet (Fig. 2H, ccf). Higher resolution of the cone cell processes (in the region between the black arrowheads, Fig. 2H) close to and near the end feet show presence of SJs as shown in Fig. 2I (black arrowheads). We also analyzed the basal region of the fenestrated membranes which rests on the basement membrane. Below the fenestrated membrane presence of extensive membrane processes from the subretinal glial cells (Fig. 2J, SRG) display extensive SJs (Fig. 2J and K, black arrowheads). Taken together our ultrastructural studies demonstrate the presence of extensive stretches of SJs between the CCs and CCs and PCs in the apical region and also near the CC feet at the bottom of the adult ommatidium. Thus the presence of SJs at the apical and basal regions of the ommatidium essentially closes the inner cavity of the PR rhabdomeres (Cagan and Ready, 1989; refer schematic in Fig. 2A).

Correlation of Nrx IV Expression with the Formation of SJs

We next performed immunofluorescence analysis to determine if the localization of SJs in the developing and adult eye coincides with the localization of known SJ-specific proteins like Nrx IV. Nrx IV has been shown to be involved in SJ formation both in epithelial cells and the nervous system (Banerjee et al., 2006; Baumgartner et al., 1996). Since the eye development involves neuronal differentiation and also the formation of non-neuronal accessory cells with dynamic rearrangements in the third larval instar, we carried out immunostaining of the third instar eye imaginal disc with anti-Nrx IV (Fig. 3A) and anti-Crumbs (Crb) (Fig. 3B). At this stage, the disc epithelial cells strongly express Nrx IV, especially in cells posterior to the morphogenetic furrow such as differentiating PRs and CCs (Fig. 3A, C). The apical domain-specific Crb protein localizes at the apical membrane in the undifferentiated cells of the retinal epithelium and the newly recruited PR cells, and seems concentrated mostly at the apical regions (Fig. 3B, C) (Izaddoost et al., 2002; Pellikka et al., 2002). Immunostaining of a late

third instar eye imaginal disc with anti-Nrx IV (Fig. 3D) and anti-chaoptin, a PR cell-specific adhesion molecule in the eye imaginal disc (24B10, Fig. 3E; Van Vactor et al., 1988) showed no overlap in the localization of the two proteins (Fig. 3F) indicating that Nrx IV is not expressed in the neuronal cells. Depending on the focal depth of the stained eye disc, Nrx IV immunoreactivity stains above or around the 24B10 positive immunoreactivity indicating that Nrx IV is expressed in the accessory cells and not the PRs.

We followed Nrx IV immunostaining into pupal development where the ommatidial cells have differentiated and their numbers have been reduced by programmed cell death and elimination (Wolff and Ready, 1991b). Immunostaining of the eye tissues around 37% of pupal development against Nrx IV and Crb showed a refined expression of Nrx IV in the CCs (white arrowhead) and PCs (white arrow, Fig. 3G) above the level of the differentiated PR rhabdomeres labeled with Crb (asterisk, Fig. 3H; see merged image I). The Crb immunoreactivity is mostly observed below the CCs. The immunoreactivity of Nrx IV in the membranes joining the CCs and the membranes of the PCs coincides with the location of the SJs (refer Fig. 1D, E). These results correlate well with the ultrastructural analysis revealing SJs between the CC membranes and between the PCs. Next we carried out immunostaining of the adult eyes in tangential orientations against Nrx IV (Fig. 3J) and Crb (Fig. 3K), which revealed that Nrx IV is strongly expressed in the membranes of the differentiated CCs (white arrowheads, Fig. 3J, L), while Crb localizes longitudinally to the rhabdomere stalk (red arrows, Fig. 3K, L; Izaddoost et al., 2002). We further carried out immunostaining of the adult eye such that the longitudinal view of the ommatidium could be visualized. Immunostaining of the adult ommatidia against Nrx IV, and Crb showed that Nrx IV is expressed by the CCs at the apical most region of the ommatidium like a cap (white arrowheads, Fig. 3M, O). Crb is expressed along the rhabdomere stalk of the PRs (red arrows, Fig. 3N, O). The immunoreactivity of Nrx IV along the length of CCs or their processes was below the level of detection. Nrx IV expression is also observed at the bottom of the CCs where the CC feet are located near the retinal floor (Fig. 3P, white arrow). In addition Nrx IV immunoreactivity is also observed at the basal regions of the secondary and tertiary PCs (Fig. 3P, FM). These basal regions contain a specialized basement membrane, the fenestrated membrane (FM) and are highly enriched in actin-based stress fiber arrays (Cagan and Ready, 1989). We also carried out immunostaining against Nrx IV in frozen sections of adult ommatidia which revealed that Nrx IV is expressed in the apical regions of the CCs (Fig. 3Q, white arrowheads), as well as at the bottom of the ommatidia highlighting the CC feet and the fenestrated membranes (Fig. 3Q, FM). Furthermore, Nrx IV is also expressed in cells at the base of the retina referred to as the subretinal glia (SRG) which also contain SJs (Fig. 3Q; Cagan and Ready, 1989; Perez and Steller, 1996). Taken together, the immunolocalization data in the larval through adult eye correlates with the presence of SJs in the apical and basal regions of the ommatidium and correlates with the presence of SJs as demonstrated by ultrastructural analysis.

Nrx IV is Not Essential for Photoreceptor Differentiation

To examine the function of Nrx IV in eye morphogenesis, we carried out somatic clonal analysis using *FLP/FRT* system (Xu and Rubin, 1993). Since the homozygous *nrx IV* null mutants are embryonic lethal, we generated loss-of-function *nrx IV* clones using two *nrx IV* null alleles (*nrx IV*^{4304} and *nrx IV*^{4025}) (Baumgartner et al., 1996). Based on the expression of Nrx IV in the precursors of CC and PCs; we predicted that these cell types would be directly affected by the loss of *nrx IV* during eye development. To investigate which aspects of ommatidial development are affected in the mutant clones, we analyzed third instar eye discs for *nrx IV* mutant clones stained for Nrx IV in combination with another primary antibody, such as, Elav, Crb, Cadherin (Cad) and Disc Large (Dlg). We found that the differentiation of PRs is unaffected in *nrx IV* mutant clones by staining eye imaginal discs with anti-ELAV antibody. As shown in Fig. (4A–C), PR determination takes place since all cells posterior to

the morphogenetic furrow (white line with double arrows) express ELAV (Fig. 4B). However, loss of Nrx IV (Fig. 4A) clearly causes a disruption of the regular ommatidial array in the mutant clone (Fig. 4C). Mutant cells do not seem to elongate properly, causing a depression in the epithelial monolayer. Since the focus is on the nuclear ELAV staining, the Nrx IV staining is slightly out of focus in these images. We next determined whether loss of Nrx IV during ommatidial development affects apico-basal polarity of the PR cells. Double labeling with anti-Nrx IV (Fig. 4D) and anti-Crb (Fig. 4E) showed that Crb is localized apically within the *nrx IV* mutant clones (Fig. 4F), suggesting that apico-basal polarity is not grossly affected although the localization pattern of Crb is not identical to that of surrounding wild-type cells. Similarly, the localization of the AJ marker, Cad (Fig 4H), (Oda et al., 1994; Tepass et al., 1996), was mostly unaltered in the mutant clones relative to the surrounding wild type cells (Fig. 4I). Based on the localization of Cad, we conclude that formation of AJs is not severely affected in the absence of Nrx IV.

Next we carried out immunostaining against a SJ protein, Dlg, that has previously been shown to be instrumental in the formation of SJs in imaginal discs (Hough et al., 1997). As shown in Fig. 4J–L, Nrx IV clones (Fig. 4J) are entirely devoid of Dlg protein (Fig. 4K; see merge in Fig. 4L). This holds true for localization of other SJ proteins, such as, Coracle (data not shown). One plausible explanation for the absence of Dlg in *nrx IV* mutant clones is that in the absence of Nrx IV, SJ proteins become unstable, are subjected to premature degradation and thus fail to show any localization in the mutant clones. This is especially true in the case of large *nrx IV* mutant clones where the tissue seems to fall out of the epithelial context towards the late third instar stages (see below). Based on these observations, we propose that mutant ommatidia initiate proper neuronal determination and differentiation, but fail to retain their proper morphology and integrity in the absence of Nrx IV.

Nrx IV is Required for Ommatidial Integrity

To determine the consequences of loss of Nrx IV on the adult ommatidia, we carried out SEM of the adult eyes with *nrx IV* mutant clones. As shown in Fig. 4M, N, large *nrx IV* mutant clones showed complete lack of ommatidia replaced by a scar-like tissue. To determine the ommatidial organization defects within small *nrx IV* mutant clones, we carried out light microscopic analysis and sectioned eyes at the level of the mutant clones which were identified by loss of the eye pigments. As shown in Fig. 4O, small *nrx IV* clones affecting few ommatidia showed relatively either normal looking ommatidia (black arrows, Fig. 4O) or ommatidia that looked fused (black arrowhead, Fig. 4O). As shown in Fig. 4P, another *nrx IV* mutant clone displays an ommatidium with no PR rhabdomeres (white arrow) or an ommatidium with reduced number of PRs or merged and abnormally shaped rhabdomeres (white arrowheads). In the large *nrx IV* mutant clones (Fig. 4Q, white line) most ommatidia in the center of the clone are missing. A more careful analysis using serial sections showed that the PRs and their rhabdomeres are often present but highly deformed. In these mutant clones the basal lamina between the PR layer and the lamina is disrupted (red line). During PR differentiation the ommatidia seem to drop out of their normal context indicating that Nrx IV is required to maintain the overall ommatidial integrity, and that it is not required for the initial differentiation of the ommatidial cells. These observations indicate that PR determination and early differentiation proceeds essentially normally in the absence of Nrx IV. During later stages of eye development loss of Nrx IV causes a failure of ommatidial adhesion or integrity, leading occasionally to the recovery of very large clones with no apparent ommatidia in the adult eye (Fig. 4M, N, Q). Based on these data, we conclude that loss of Nrx IV does not affect PR determination but causes a collapse of differentiating PR cells and ommatidia during later stages of eye development.

nrx IV$^{-/-}$ Mutant Ommatidia Display Loss of Cone Cell SJs and Undergo Photoreceptor Degeneration

The light microscopic analysis of *nrx IV*$^{-/-}$ mutant clones that spanned several ommatidia revealed collapse of the entire ommatidial units. While on one hand, these studies provided insights into the requirement of Nrx IV in ommatidial integrity, they did not allow us to visualize the precise defects that resulted when Nrx IV was lost from a single ommatidium. We, therefore, performed ultrastructural analysis of a single ommatidium that was mutant for Nrx IV. Low magnification images of a longitudinal section through a wild type adult eye at the level of the pseudocone cavity (psc) and CCs shows the normal ommatidial organization (Fig. 5A). Note the well-formed rhabdomeres that stretch downwards. The PCs are also visible flanking the CCs. A longitudinal section at a comparable level of a *nrx IV* mutant ommatidium (Fig. 5B) shows somewhat stunted CCs and shorter rhabdomeres. The pseudocone cavity is flanked by PCs that lack pigment granules. At a higher magnification, membranes between the CCs in the wild type and mutant ommatidia are evident (black arrowheads, Fig. 5C, D). The stunted shape of CCs and rhabdomeres is clear in *nrx IV* mutant ommatidium (compare 5C with 5D). At higher magnification, the ladder-like SJs between wild type CC membranes are clearly visible (black arrows Fig. 5E, G) along with the AJs (white arrow, Fig. 5E). In the mutant ommatidium (Fig. 5F, H), the ladder-like SJs between the CC membranes are completely absent (black arrows). However, the CC membranes show normal spacing with apical AJs similar to their wild type counterpart (white arrow, Fig. 5F, H). Thus the ultrastructural analysis of *nrx IV* mutant ommatidia demonstrates that loss of Nrx IV results in the specific loss of SJs between the CCs.

The light microscopic and ultrastructural studies of *nrx IV* mutant ommatidia showed a variety of defects in the ommatidial morphology and integrity due to loss of Nrx IV in the accessory CC and PCs. A cross section through an adult eye in the apical region shows many wild type PR clusters surrounded by PCs (Fig. 6A). In the center of the wild type ommatidia is a *nrx IV* mutant clone lacking pigment granules with abnormally shaped and fused rhabdomeres (black arrowheads, Fig. 6A). At a higher magnification, the wild type PR rhabdomeres show a perfect trapezoid arrangement (Fig. 6B). This arrangement of PR rhabdomeres is abolished in the *nrx IV* mutant ommatidia. The mutant ommatidia display fused and abnormal rhabdomeres (Fig. 6C). As seen at a much higher magnification, the wild type PR stalks are linked by characteristic AJs (black arrowhead, Fig. 6D; Izaddoost et al., 2002;Pellikka et al., 2002). The rhabdomeres in *nrx IV* mutant ommatidia display many abnormal anatomical features including fused stalkless rhabdomeres, and a total disarray of overall PR organization (black arrows, Fig. 6). In addition, PR degeneration and disorganization was a common feature in small *nrx IV* clones (Fig. 6F, G). Surprisingly, the degenerated PRs (asterisk, Fig. 6G) displayed a long stretch of AJs near their stalks (Fig. 6G, black arrowheads). Taken together, these ultrastructural findings highlight an essential role of the accessory cells and their SJs in the organization and/ or maintenance of the PR clusters in the adult ommatidia. These findings further support the idea that the CC and PCs serve as a special type of glial cells to protect the ion and light sensitive PRs during and after their development (see Discussion).

The Blood-Eye Barrier Function is Compromised in *nrx IV* Hypomorphic Mutants

Carlson et al. (1998) reported that a functional BEB is established during pupal eye development that allows the differentiating light-sensitive PRs to maintain an ionic microenvironment that is conducive for phototransduction. To determine whether mutations in *nrx IV* compromised this BEB function in adult eyes we selected *nrx IV* hypomorphic alleles reported previously (Baumgartner et al., 1996). We first determined the precise molecular defects in three *nrx IV* alleles which expressed the mutant Nrx IV protein (Baumgartner et al., 1996). A cartoon depicting the primary structure and domain organization of Nrx IV is shown in Fig. 7A along with the molecular lesions in *nrx IV* alleles *711*, *2511* and *319*. Two *nrx IV*

alleles *319* and *711* show missense mutations in two different laminin G domains. The amino acids that have been mutated in each of the laminin G domains are conserved between the Neurexin IV family members (Bellen et al., 1998), suggesting an important functional role for the Laminin G domains and more specifically for these specific amino acids. *nrx IV* allele *2511* showed a 61 nucleotide deletion in an intron without causing truncation in Nrx IV protein. Immunostaining of wild type (Fig. 7B) and *nrx IV* alleles *319* (Fig. 7C), *711* (Fig. 7D) and *2511* (Fig. 7E) with anti-Nrx IV (green) and anti-Crb (red) revealed that all these three alleles express Nrx IV. However, the localization of Nrx IV at the SJs is more basal and diffuse (white arrowheads, compare C–E with B). Interestingly, the apico-basal polarity is not compromised in any of these *nrx IV* mutants (Fig. 7C–E), as Crb localizes to the apical domain similar to the wild type embryos (Fig. 7B). The null and hypomorphic alleles of *nrx IV* are embryonic lethal, however, transheterozygous hypomorphic alleles produce weak adults at a very low frequency. The adult flies that emerged from crosses between *nrx IV*^{319}, *nrx IV*^{711} and *nrx IV*^{2511} were first analyzed by SEM to determine the overall eye morphology. As shown in Fig. 7G–I, the adult eyes of *nrx IV*$^{319/711}$ (Fig. 7G), *nrx IV*$^{711/2511}$ (Fig. 7H) and *nrx IV*$^{319/2511}$ (Fig. 7I) were indistinguishable from those of the wild type at this magnification (Fig. 7F), except that occasionally a bristle or two were found missing in the mutant combinations. The normal eye morphology and the fact that Nrx IV is expressed in these alleles prompted us to determine the adult ommatidial morphology using immunofluorescence against Nrx IV. As shown in Fig. 7K–M, Nrx IV is expressed in the eyes of all the mutant combinations, but the localization of Nrx IV is abnormal compared to the wild type (Fig. 7J). Wild type Nrx IV localizes sharply to the CC and PC membranes (Fig. 7J), while the mutant Nrx IV protein in *nrx IV*$^{319/711}$ (Fig. 7K), *nrx IV*$^{711/2511}$ (Fig. 7L) and *nrx IV*$^{319/2511}$ (Fig. 7M) shows diffuse localization and/or a reduction in the levels of the Nrx IV protein. In fact, there is a gradation of the phenotype between these allelic combinations with *nrx IV*$^{319/2511}$ being the most severe and *nrx IV*$^{319/711}$ appearing to be the least severe. These data suggest that the hypomorphic *nrx IV* mutants fail to localize Nrx IV precisely at the SJs.

To determine whether these hypomorphic mutant adult flies presented a defective BEB, we carried out in vivo diffusion barrier assays to see whether a 3kDa molecular weight FITC-dextran dye would penetrate into the brain or the retinal areas due to a breach of the barrier as has been previously reported for *moody* and *nrx IV* mutants (Bainton et al., 2005; Banerjee et al., 2006). As shown in Fig. 7O–Q, the FITC-dextran dye shows a gradation in the retinal dye accumulation compared to the wild type (Fig. 7N). The dye accumulation at varying levels in *nrx IV*$^{319/711}$ (Fig. 7O), *nrx IV*$^{711/2511}$ (Fig. 7P) and *nrx IV*$^{319/2511}$ (Fig. 7Q) also reflected the severity of Nrx IV mislocalization and ommatidial disorganization.

Since the dye penetration in the entire whole mount adult eye gives a qualitative assessment of the breach of the barrier, we carried out a semiquantitative analysis of the dye penetration in *nrx IV* hypomorphic allelic combinations. The fluorescent dye penetration estimates were performed on multiple brains controlling for anatomic location and depth of confocal images (*refer Methods for details*). Confocal analysis of the cuticle bare heads revealed increasing penetration of the dye into increasingly severe *nrx IV* hypomorphs (compare Fig. 7S–U with control in Fig. 7R). In the wild type control heads, the dye stops at the retina (R) and lamina (L) boundary as well as at the L and lobular plate (LP) interface (Fig. 7R). Compared to the wild type controls (which were set at background levels +/− (Fig. 7R), *nrx IV* hypomorphic combinations showed increasing dye penetration which correlated with the severity of the phenotype observed in the whole eye dye penetration assays (Fig. 7S–U). Fluorescence intensity measurements of the hypomorphs estimated *nrx IV*$^{319/711}$ with 12–18 units (+; Fig. 7S), *nrx IV*$^{2511/711}$ with 30–40 units (++; Fig. 7T) and *nrx IV*$^{319/2511}$ with 60–90 units (+++; Fig. 7U). The most severe allelic combination *nrx IV*$^{319/2511}$ again displayed a strong dye penetration phenotype as seen with whole mount eyes. Note that the ommatidia of the *nrx IV*$^{319/2511}$ eyes are highlighted in the retina by the dye that has reached the apical areas (Fig.

7U, arrowheads). These data strongly suggest that the hypomorphic mutant combinations of *nrx IV* result in an aberrant retinal barrier function and that SJs are important in maintaining a functional BEB in *Drosophila*.

Aberrant Ultrastructure of SJs in *nrx IV* Hypomorphic Alleles

One of the advantages of generating EMS-induced mutations is the recovery of single amino acid changes in the proteins due to single nucleotide changes. These amino acid changes often result in loss of function of proteins. As presented in the preceding sections that hypomorphic alleles of *nrx IV* produce proteins that have single amino acid changes (Fig. 7A), display mislocalization at the SJs (Fig. 7B) and also show a breach of the BEB (Fig. 7N–U). We wanted to determine whether these amino acid changes result in ultrastructural defects in the SJ organization and morphology. Electron microscopic examination of the cross sections of adult eyes from the most severe *nrx IV* hypomorphic allelic combination ($nrx\ IV^{319/2511}$) showed that overall morphology of ommatidium is preserved at the level of the CCs. All four CCs are present and display presence of junctional structures at the CC interface (Fig. 8A, black arrowheads). At a higher magnification the CC –CC SJs display less discrete junctional organization (Fig. 8B, black arrowheads). Note that the structure of the AJs between the CCs is not altered (Fig. 8B, black arrows). Next we analyzed the longitudinal sections of the *nrx IV* hypomorphic mutant ommatidia which again revealed a normal tissue organization with the presence of CCs and PR rhabdomeres (Fig. 8C, Rb) but the SJs between CC again displayed a less structured appearance (Fig. 8C, black arrowheads). At a higher magnification, the morphological changes in the SJ structure between the CCs are more evident (Fig. 8D, black arrowheads). We also analyzed the anatomical organization in the basal regions of the mutant ommatidia. As shown in Fig. 8E, F, the mutant ommatidia displayed normal cellular organization with the fenestrated membranes at the base of the ommatidia (FM).

In the more basal region from the fenestrated membrane, a tracheal branch (Tr) and the layer of subretinal glia are also present (Fig. 8E, F). Thus, the ultrastructural analysis of the *nrx IV* hypomorphic mutant combinations revealed a normal cellular organization but defective SJ structure, which underlies the breach of the BEB observed in the hypomorphic mutants. Taken together, the null and hypomorphic *nrx IV* mutant phenotypes provide clues about the structure/function role of Nrx IV in the biogenesis of SJs.

Discussion

In the present study, we analyzed developing and adult *Drosophila* ommatidia for the presence and location of SJs. We show that SJs are present in the retinal epithelial cells in the imaginal discs, pupal eye discs and the adult ommatidia. In the adult ommatidia these junctions are specifically located in the apical and basal regions between the CCs, between the PCs and between the CCs and PCs. We also showed that the localization of Nrx IV, a SJ specific protein, coincides with the location of SJs during key stages of eye development. Taking advantage of the *nrx IV* null and hypomorphic mutants, we were able to show that SJs are essential for ommatidial integrity and BEB function. Our studies in the future will allow a structure/function analysis of the organization and function of SJs in an adult *Drosophila* organ that provides a read out of the signaling abnormalities during its development and is not crucial for the survival of the organism.

Intercellular Junctions and Ommatidial Organization

Previous studies on the eye development have established the fate map of various cell types that form an adult ommatidium (Cagan and Ready, 1989; Tomlinson and Ready, 1987; reviewed in Wolff and Ready, 1993). While the anatomy and placement of cell types that include neuronal PRs and accessory CCs and PCs is well worked out, the junctional

organization between these cell types remains to be elucidated. Specialized areas of contacts between adjacent cell membranes are extremely important for proper cellular assembly and tissue organization (Bao and Cagan, 2005). Among the junctional components typical of any polarized epithelia, AJs have been characterized in greater detail in the *Drosophila* ommatidia (Frohlich, 2001; Izaddoost et al., 2002; Laprise et al., 2006; Pellikka et al., 2002). The AJs demarcate the apical and basal domains, contribute to intercellular adhesion and are coupled with the cytoskeleton. The AJs also serve as sites for many signal transduction pathways (Kirkpatrick and Peifer, 1995).

We hypothesize that the presence of SJs between and among the CCs and PCs in the adult *Drosophila* ommatidia function to maintain proper adhesion between many cell types. The presence of rhabdomeres in the lamina in large *nrx IV* clones suggests that the ommatidia fail to hold together either due to loss of adhesion at the apical and basal ends of the ommatidia or due to defective stretching during ommatidial development. These misplaced rhabdomere phenotypes are only observed in large clones. Small *nrx IV* mutant clones display fused or abnormally structured rhabdomeres suggesting that proper junctional organization between the cells is essential for ommatidial integrity. The immunofluorescence analysis of Nrx IV revealed that within the eye discs Nrx IV is enriched in the CC and PC precursors and found at much reduced levels in the PR precursors. This unequal distribution in different cell types in the eye imaginal tissues correlates with the distribution pattern of SJs in the *Drosophila* ommatidia. In *Musca*, SJs have been located between CCs and between the CCs and PCs (Chi and Carlson, 1976). Although a SJ marker in *Musca* has not been molecularly identified, homologs of *Drosophila* SJ proteins are likely to localize at the *Musca* eye SJs. Thus, our current findings indicate that the dynamic profile of Nrx IV localization corresponds to the location of SJs in the developing and adult ommatidium.

Contribution of Non-neuronal Accessory cells to Ommatidial Integrity

During ommatidial development, the earliest cell types that are specified are the PRs during the larval third instar (Tomlinson and Ready, 1987). The accessory CC and PC specification follows that of the PRs. During pupal development, the newly established cellular units stretch longitudinally to become an ommatidium. All cells establish a unique relationship with each other and with the PRs encased in the core of the ommatidium. The CC and PCs transform into long, slender chord-like cellular extensions that descend down to the retinal floor providing a vertical framework around the ommatidium. This network of lateral processes mechanically strengthens the unit, imparting a three-dimensional stability and integrity and optically insulates the PR rhabdomeres. In general terms, the entire ommatidium must be well suspended from the lens and the lateral processes of the accessory cells to help maintain constant spacing of the PR unit, ensuring their optical alignment. Not just vertically, the different types of PC membranes are connected horizontally as well, reinforcing support and stability.

The CC and PCs have long been classified as accessory cell types of the ommatidial unit (Cagan and Ready, 1989; Wolff and Ready, 1993). Studies on Sparkling function hypothesized that CCs might be considered as glial cells that support the PR neurons (Fu and Noll, 1997). The present study further strengthens that CCs and PCs share similarities with the glial cells of the *Drosophila* nervous system as they strongly express SJ-specific glial protein, Nrx IV and that these cell types have SJs similar to the glial cells in the nervous system (Banerjee et al., 2006). Finally, CCs and PCs are non-neuronal accessory cells to the PR neurons and perform an ensheathment function around the PRs (Cagan and Ready, 1989). This ensheathment function may be critical to the physiological changes that occur during phototransduction in the adult ommatidium.

At the bottom of the ommatidium, the retinal floor has specialized structures. The CC processes end into bulb-shaped end feet and the basal most ends of the secondary and tertiary PCs

transform into a unique anatomical structure, the fenestrated membrane. In between the CC feet and the fenestrated membranes, distinct holes or ports are created through which the PR axon bundles project into the lamina area. Similar to AJs, focal adhesions are reported to surround the axon-exiting areas at the retinal floor (Longley and Ready, 1995). It is possible that the fenestrated regions function as an anchor at the base holding the elongated ommatidial unit upright and together with CC feet seal the optical unit at the base of the ommatidia. Our finding that Nrx IV is localized to CC feet and the fenestrated membrane and the presence of SJs near the CC feet, further strengthens the idea that SJs are required to create an ionic microenvironment to protect the light and ion sensitive PR rhabdomeres in the adult ommatidia, as has been previously proposed (Shaw, 1978; reviewed in Carlson et al., 2000).

SJs and Photoreceptor Degeneration

The findings that the PR rhabdomeres fuse and that PRs degenerate in the absence of Nrx IV raises several interesting issues concerning the direct and indirect consequences of the loss of Nrx IV and SJs in the CCs and PCs. Since Nrx IV is not expressed in the wild type PRs, the degeneration of PRs observed in *nrx IV* clones and their altered cellular and junctional morphology are probably due to secondary consequences. Loss of Nrx IV function from the non-neuronal CC and PCs may lead to structural alterations and lack of proper cell-cell adhesion leading to misalignment of PRs. Since the CC processes taper as they reach towards the base of the ommatidia and form rounded protrusions, the CC feet (Longley and Ready, 1995; Wolff and Ready, 1993), disruption of this structure could also misplace the PRs leading to their degeneration. Alternatively, Nrx IV at the SJs may play additional non-structural roles like signaling between PRs and CC and PCs to maintain PR survival. Similar PR degeneration phenotypes have been reported in *sparkling* mutants when Sparkling is lost from the precursors of the CCs (Fu and Noll, 1997). A mutual dependence between neurons and non-neuronal glial cells is not uncommon in the nervous system. Not just in the context of the eye, but there are numerous examples of interdependence between neuronal and glial cells for mutual survival and bidirectional signaling in the nervous system (Bhat, 2003; Sepp and Auld, 2003).

Ommatidial Development and Blood-Eye Barrier Function

The presence of SJs in the adult ommatidium can play dual functions: one to provide cell adhesion and thus mechanical strength and second to create an ionic or molecular barrier. Thus SJs can provide both the adhesive and barrier functions for the encased PRs from the top and the bottom. Although the functional correlates of this barrier are well known in the mammalian systems, the establishment or the maintenance of the blood-retinal barrier in the *Drosophila* eye remains to be investigated. The breach of the BEB in *nrx IV* hypomorphic allelic combinations suggests that a barrier system exists in the eye. How this barrier system allows the photosensitive rhabdomeres to function during phototransduction is not clear. Since *Drosophila* PR rhabdomeres trap axially directed light, a stable ionic microenvironment may help reduce the noise or variations in phototransduction and this can be only possible if a barrier is maintained around the rhabdomeres. As presented in Fig. 7R–U, in the wild type heads, no dye seems to pass the lobular plate/lamina and lamina/retina boundaries and the levels of the dye present is below detection limits within the tissues. This suggests that a barrier system exists at these boundaries. Interestingly, in *nrx IV* hypomorphic mutant combinations, the dye breaches through the barrier at varying degrees with most severe hypomorphic combination displaying the highest level of the breach (Fig. 7U). These findings suggest that a barrier system exists at the bottom of the ommatidia but do not rule out the role of the apical junctions in the barrier function. Similarly, the presence of the dye in the ommatidia in the most severe hypomorphs shows that the dye has penetrated all the way into the apical regions of the ommatidia. This is consistent with the ultrastructural analysis of these mutants where we observed normal cellular organization but aberrant ultrastructure of the SJs, which leads to the breach of the barrier. Thus functional SJs are essential for BEB integrity and defects in SJ

structure lead to a breakdown of the BEB system. Furthermore, the hypomorphic phenotypes suggest that the mutant Nrx IV proteins retain some of the functions at least the adhesive properties but fail to maintain the barrier function based on the fact that the ommatidial organization is not disrupted. These observations highlight important aspects of the SJ protein functions where individual domains of these proteins may be involved in specific protein-protein interactions during SJ biogenesis. Such phenotypes have been observed in *moody* flies, which also lack the barrier function of the SJs but the adhesive properties are retained (Bainton et al., 2005; Schwabe et al., 2005).

In insects, such as *Musca* TJs are known to exist between marginal glia at the base of the lamina, which might be a basis of a lamina-medulla barrier (Carlson et al., 1998; Saint Marie and Carlson, 1983a; Saint Marie and Carlson, 1983b). It is unlikely that TJs in the lamina layer play any appreciable role in the blood-eye barrier formation, as the barrier exists at the retinal floor where SJs are observed. Our observations are consistent with those of Shaw (1978), which suggest that a blood-eye barrier is established by the SJs in the insects. In *Drosophila*, there might also be additional barriers below the basement membrane down to the underlying lamina and medulla layers formed by a variety of glial cells that inhabit these layers and ensheath the PR axons. Existence of such a barrier below the basement membrane has been suggested in the housefly and locust eyes (Chi and Carlson, 1981; Shaw, 1978). In the future, manipulation of the junctional organization coupled with the electrophysiological measurements may provide insights into how SJs are involved in creating a functional blood-eye or blood-retinal barrier in the *Drosophila* eye. The classical and most widely studied role of SJs has been in the paracellular barrier formation and function during embryonic development (Auld et al., 1995; Banerjee et al., 2006; Baumgartner et al., 1996). A compromise in the integrity of the vertebrate BRB due to breakdown of the occluding junctional architecture is the underlying basis of many pathologies, with still poorly understood cellular mechanisms (Vinores, 1995; Banerjee and Bhat, 2007). Understanding the molecular organization of a barrier system in the adult *Drosophila* eye may be more advantageous as a functional read out could be assessed by the dye-penetration assay as well as electrophysiological methods to monitor phototransduction. In conclusion, our studies establish the presence and novel functions of SJs in the *Drosophila* eye. The characterization of Nrx IV function during eye development has provided a glimpse into some of the important aspects of cellular events in ommatidial development. Future studies may provide additional insights into whether the SJs, in addition to providing structural integrity and barrier function, play a much broader role in intercellular communication between neuronal PRs and glia-like CCs and PCs.

Acknowledgements

We thank H. J. Bellen and K. W. Choi for their suggestions; R. Fehon, T. Uemura, P. Bryant and DSHB for various reagents and V. Madden of the UNC-EM Core for technical assistance. We are grateful to D. Ready for allowing us to use the schematic shown in Fig. 2A and A. Vaseva for drawing this schematic. We also thank anonymous reviewers for their insightful comments which lead to significant improvements in the data presented here. This work was supported by the National Institutes of Health grants GM63074 and NS050356 (M.A.B.) and funds from the State of North Carolina.

References

Auld VJ, Fetter RD, Broadie K, Goodman CS. Gliotactin, a novel transmembrane protein on peripheral glia, is required to form the blood-nerve barrier in Drosophila. Cell 1995;81:757–767. [PubMed: 7539719]

Bainton RJ, Tsai LT, Schwabe T, DeSalvo M, Gaul U, Heberlein U. moody encodes two GPCRs that regulate cocaine behaviors and blood-brain barrier permeability in Drosophila. Cell 2005;123:145–156. [PubMed: 16213219]

Banerjee S, Pillai AM, Paik R, Li J, Bhat MA. Axonal ensheathment and septate junction formation in the peripheral nervous system of Drosophila. J Neurosci 2006;26:3319–3329. [PubMed: 16554482]

Banerjee S, Bhat MA. Neuron-glial interactions in blood-brain barrier formation. Annu Rev Neurosci 2007;30:235–258. [PubMed: 17506642]

Bao S, Cagan R. Preferential adhesion mediated by Hibris and Roughest regulates morphogenesis and patterning in the Drosophila eye. Dev Cell 2005;8:925–935. [PubMed: 15935781]

Baumgartner S, Littleton JT, Broadie K, Bhat MA, Harbecke R, Lengyel JA, Chiquet-Ehrismann R, Prokop A, Bellen HJ. A Drosophila neurexin is required for septate junction and blood-nerve barrier formation and function. Cell 1996;87:1059–1068. [PubMed: 8978610]

Behr M, Riedel D, Schuh R. The claudin-like megatrachea is essential in septate junctions for the epithelial barrier function in Drosophila. Dev Cell 2003;5:611–620. [PubMed: 14536062]

Bhat MA. Molecular organization of axo-glial junctions. Curr Opin Neurobiol 2003;13:552–559. [PubMed: 14630217]

Bhat MA, Izaddoost S, Lu Y, Cho KO, Choi KW, Bellen HJ. Discs Lost, a novel multi-PDZ domain protein, establishes and maintains epithelial polarity. Cell 1999;96:833–845. [PubMed: 10102271]

Blochlinger K, Jan LY, Jan YN. Postembryonic patterns of expression of cut, a locus regulating sensory organ identity in Drosophila. Development 1993;117:441–450. [PubMed: 8330519]

Cagan RL, Ready DF. The emergence of order in the Drosophila pupal retina. Dev Biol 1989;136:346–362. [PubMed: 2511048]

Carlson SD, Hilgers SL, Garment MB. Blood-eye barrier of the developing Drosophila melanogaster Diptera: Drosophilidae. Int J Insect Morphol & Embryol 1998;27:241–247.

Carlson SD, Juang JL, Hilgers SL, Garment MB. Blood barriers of the insect. Annu Rev Entomol 2000;45:151–174. [PubMed: 10761574]

Chen R, Amoui M, Zhang Z, Mardon G. Dachshund and eyes absent proteins form a complex and function synergistically to induce ectopic eye development in Drosophila. Cell 1997;91:893–903. [PubMed: 9428513]

Chi C, Carlson SD. The large pigment cell of the compound eye of the house fly Musca domestica. Fine structure and cytoarchitectural associations. Cell Tissue Res 1976;170:77–88. [PubMed: 949735]

Chi C, Carlson SD. The perineurium of the adult housefly: ultrastructure and permeability to lanthanum. Cell Tissue Res 1981;217:373–386. [PubMed: 7237533]

Faivre-Sarrailh C, Banerjee S, Li J, Hortsch M, Laval M, Bhat MA. Drosophila contactin, a homolog of vertebrate contactin, is required for septate junction organization and paracellular barrier function. Development 2004;131:4931–4942. [PubMed: 15459097]

Frohlich A. A scanning electron-microscopic study of apical contacts in the eye during postembryonic development of Drosophila melanogaster. Cell Tissue Res 2001;303:117–128. [PubMed: 11235999]

Fu W, Noll M. The Pax2 homolog sparkling is required for development of cone and pigment cells in the Drosophila eye. Genes Dev 1997;11:2066–2078. [PubMed: 9284046]

Halder G, Callaerts P, Flister S, Walldorf U, Kloter U, Gehring WJ. Eyeless initiates the expression of both sine oculis and eyes absent during Drosophila compound eye development. Development 1998;125:2181–2191. [PubMed: 9584118]

Hardie RC, Raghu P. Visual transduction in Drosophila. Nature 2001;413:186–193. [PubMed: 11557987]

Hayashi T, Kojima T, Saigo K. Specification of primary pigment cell and outer photoreceptor fates by BarH1 homeobox gene in the developing Drosophila eye. Dev Biol 1998;200:131–145. [PubMed: 9705222]

Higashijima S, Kojima T, Michiue T, Ishimaru S, Emori Y, Saigo K. Dual Bar homeo box genes of Drosophila required in two photoreceptor cells, R1 and R6, and primary pigment cells for normal eye development. Genes Dev 1992;6:50–60. [PubMed: 1346120]

Hough CD, Woods DF, Park S, Bryant PJ. Organizing a functional junctional complex requires specific domains of the Drosophila MAGUK Discs large. Genes Dev 1997;11:3242–3253. [PubMed: 9389655]

Izaddoost S, Nam SC, Bhat MA, Bellen HJ, Choi KW. Drosophila Crumbs is a positional cue in photoreceptor adherens junctions and rhabdomeres. Nature 2002;416:178–183. [PubMed: 11850624]

Kirkpatrick C, Peifer M. Not just glue: cell-cell junctions as cellular signaling centers. Curr Opin Genet Dev 1995;5:56–65. [PubMed: 7749327]

Kumar JP, Ready DF. Rhodopsin plays an essential structural role in Drosophila photoreceptor development. Development 1995;121:4359–4370. [PubMed: 8575336]

Lane, NJ. Tight junctions in invertebrates. In: Cereijido, M.; Anderson, J., editors. Tight Junctions. 2. CRC Press; New York: 2001. p. 39-59.

Laprise P, Beronja S, Silva-Gagliardi NF, Pellikka M, Jensen AM, McGlade CJ, Tepass U. The FERM protein Yurt is a negative regulatory component of the Crumbs complex that controls epithelial polarity and apical membrane size. Dev Cell 2006;11:363–374. [PubMed: 16950127]

Longley RL Jr, Ready DF. Integrins and the development of three-dimensional structure in the Drosophila compound eye. Dev Biol 1995;171:415–433. [PubMed: 7556924]

Mardon G, Solomon NM, Rubin GM. dachshund encodes a nuclear protein required for normal eye and leg development in Drosophila. Development 1994;120:3473–3486. [PubMed: 7821215]

Oda H, Uemura T, Harada Y, Iwai Y, Takeichi M. A Drosophila homolog of cadherin associated with armadillo and essential for embryonic cell-cell adhesion. Dev Biol 1994;165:716–726. [PubMed: 7958432]

Pellikka M, Tanentzapf G, Pinto M, Smith C, McGlade CJ, Ready DF, Tepass U. Crumbs, the Drosophila homologue of human CRB1/RP12, is essential for photoreceptor morphogenesis. Nature 2002;416:143–149. [PubMed: 11850625]

Peng S, Rahner C, Rizzolo LJ. Apical and basal regulation of the permeability of the retinal pigment epithelium. Invest Ophthalmol Vis Sci 2003;44:808–817. [PubMed: 12556417]

Perez SE, Steller H. Migration of glial cells into retinal axon target field in Drosophila melanogaster. J Neurobiol 1996;30:359–373. [PubMed: 8807529]

Ranganathan R, Malicki DM, Zuker CS. Signal transduction in Drosophila photoreceptors. Annu Rev Neurosci 1995;18:283–317. [PubMed: 7605064]

Saint Marie RL, Carlson SD. The fine structure of neuroglia in the lamina ganglionaris of the housefly, Musca domestica L. J Neurocytol 1983a;12:213–241. [PubMed: 6842275]

Saint Marie RL, Carlson SD. Glial membrane specializations and the compartmentalization of the lamina ganglionaris of the housefly compound eye. J Neurocytol 1983b;12:243–275. [PubMed: 6842276]

Schwabe T, Bainton RJ, Fetter RD, Heberlein U, Gaul U. GPCR signaling is required for blood-brain barrier formation in Drosophila. Cell 2005;123:133–144. [PubMed: 16213218]

Sepp KJ, Auld VJ. Reciprocal interactions between neurons and glia are required for Drosophila peripheral nervous system development. J Neurosci 2003;23:8221–8230. [PubMed: 12967983]

Shaw SR. The extracellular space and blood-eye barrier in an insect retina: an ultrastructural study. Cell Tissue Res 1978;188:35–61. [PubMed: 639096]

Smith, RS., editor. Systematic evaluation of the mouse eye. CRC Press; New York: 2002.

Tepass U, Gruszynski-DeFeo E, Haag TA, Omatyar L, Torok T, Hartenstein V. shotgun encodes Drosophila E-cadherin and is preferentially required during cell rearrangement in the neurectoderm and other morphogenetically active epithelia. Genes Dev 1996;10:672–685. [PubMed: 8598295]

Tepass U, Hartenstein V. The development of cellular junctions in the Drosophila embryo. Dev Biol 1994;161:563–596. [PubMed: 8314002]

Tepass U, Tanentzapf G, Ward R, Fehon R. Epithelial cell polarity and cell junctions in Drosophila. Annu Rev Genet 2001;35:747–784. [PubMed: 11700298]

Tomlinson A. Cellular interactions in the developing Drosophila eye. Development 1988;104:183–193. [PubMed: 3076112]

Tomlinson A, Ready DF. Cell fate in the Drosophila Ommatidium. Dev Biol 1987;123:264–275. [PubMed: 17985474]

Van Vactor D, Krantz DE, Reinke R, Zipursky SL. Analysis of mutants in chaoptin, a photoreceptor cell-specific glycoprotein in Drosophila, reveals its role in cellular morphogenesis. Cell 1988;52:281–290. [PubMed: 2449286]

Vinores SA. Assessment of blood-retinal barrier integrity. Histol Histopathol 1995;10:141–154. [PubMed: 7756735]

Vinores SA, Derevjanik NL, Ozaki H, Okamoto N, Campochiaro PA. Cellular mechanisms of blood-retinal barrier dysfunction in macular edema. Doc Ophthalmol 1999;97:217–228. [PubMed: 10896335]

Williams CD, Rizzolo LJ. Remodeling of junctional complexes during the development of the outer blood-retinal barrier. Anat Rec 1997;249:380–388. [PubMed: 9372172]

Wolff T. EGF receptor signaling: putting a new spin on eye development. Curr Biol 2003;13:R813–814. [PubMed: 14561424]

Wolff T, Ready DF. The beginning of pattern formation in the Drosophila compound eye: the morphogenetic furrow and the second mitotic wave. Development 1991a;113:841–850. [PubMed: 1726564]

Wolff T, Ready DF. Cell death in normal and rough eye mutants of Drosophila. Development 1991b; 113:825–839. [PubMed: 1821853]

Wolff, T.; Ready, DF. Pattern formation in the Drosophila retina. In: Bate, M.; Arias, AM., editors. The Development of Drosophila melanogaster. II. Cold Spring Harbor Laboratory Press; New York: 1993. p. 1277-1325.

Wu VM, Schulte J, Hirschi A, Tepass U, Beitel GJ. Sinuous is a Drosophila claudin required for septate junction organization and epithelial tube size control. J Cell Biol 2004;164:313–323. [PubMed: 14734539]

Xu T, Rubin GM. Analysis of genetic mosaics in developing and adult Drosophila tissues. Development 1993;117:1223–1237. [PubMed: 8404527]

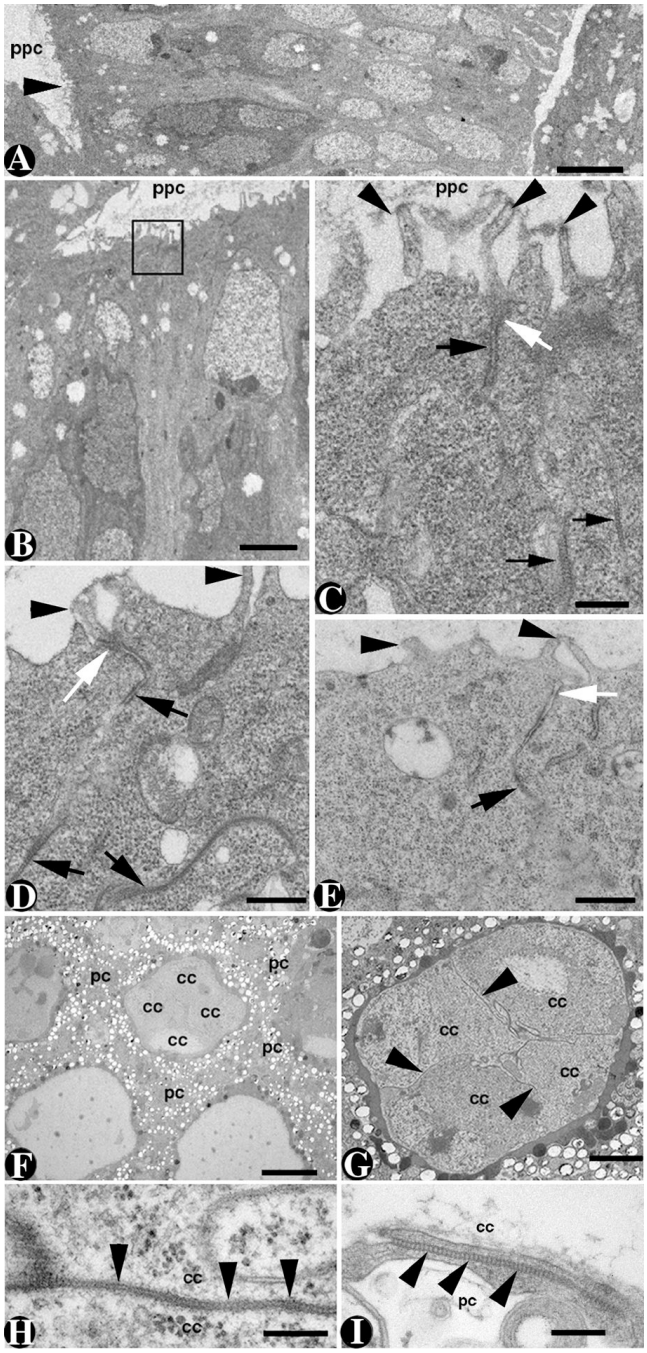

Figure 1. Spatiotemporal localization of SJs during eye development

(A) A transmission electron micrograph of a longitudinal section through a third-instar eye imaginal disc shows an apical-basal view of the cells in the disc epithelium (apical is left, anterior is top). The morphogenetic furrow (*not shown*) is about 4 ommatidial units towards the top of the section. The microvilli in the apical region project into the peripodial cavity (ppc). The black arrowhead points to a region magnified in panel B. (B) Higher magnification of the apical region shows microvilli facing the ppc (apical is top). (C) Higher magnification of the boxed area in B shows the presence of microvilli (black arrowheads), AJs (white arrow) and short stretches of SJs in the basolateral regions of the disc epithelial cells (black arrows). (D, E) Electron micrographs of longitudinal sections through early pupal eye discs show the

presence of microvilli (black arrowheads), AJs between the apical regions of the ommatidial cells below the microvilli (white arrow) and stretches of SJs (black arrows). (F) A lower magnification of a cross-section through an adult eye reveals the presence of four CCs (cc) surrounded by the PCs (pc) as evident from the pigment granules. (G) A higher magnification of a CC cluster just below the level of the pseudocone from a single ommatidium in cross-section shows the presence of 4 CCs. The electron dense lines represent the membrane interfaces between the CCs (black arrowheads). Surrounding the CC cluster are the PCs. (H) A higher magnification of a portion of the CC membranes show the presence of extensive SJs (black arrowheads). (I) Distinct ladder like SJs are also observed between the CC and PC membranes that surround the CCs (arrowheads). Scale bars: A, F, 5μm; B, 2.5μm, C–E, 0.5μm; G, 2μm; H, I, 0.2μm.

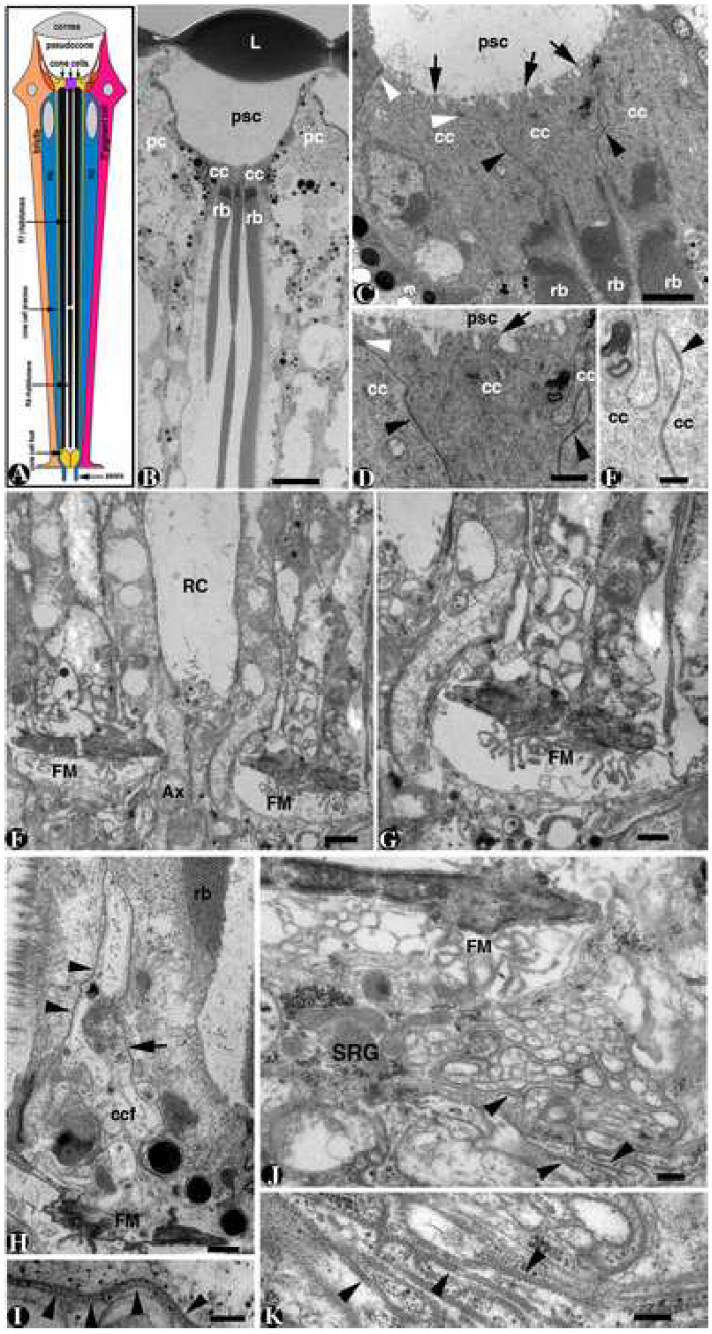

Figure 2. Various cell types and the location of SJs in the adult ommatidium

(A) A classic schematic of a longitudinal view of an adult ommatidium elucidating the various cell types: PRs, CC and PCs (modified with permission from CSHL Press; Cagan and Ready, 1989; Wolff and Ready, 1993). Note that 3 CCs below the pseudocone chamber are seen surrounded by the primary PCs. (B) Electron micrograph of a longitudinal section through an adult ommatidium in the apical half reveals the presence of corneal lens (L) on top of pseudocone cavity (psc) bordered by the primary PCs (pc). CCs (cc) are present below the pseudocone chamber which extend their processes to the CC feet at the floor of the retinal plate. The PR rhabdomeres cut longitudinally are also visible. (C) Electron micrograph of a longitudinal section through an adult ommatidium at a higher magnification shows the presence

of microvilli (black arrows) protruding into the pseudocone cavity (psc). The CCs are separated by CC membrane that have apical AJs (white arrowheads) and basolateral SJs (black arrowheads). The rhabdomeres (rb) are present below the CCs (see schematic in A). (D–E) At a higher magnification, long stretches of ladder-like SJs (black arrowheads) are observed between the CC membranes in the ommatidia. Note the CC membrane folds that contain SJs (black arrowheads, E). (F) Electron micrograph showing the basal region or the retinal floor with the PC endings that form the fenestrated membranes (FM) flanking the exit points of the PR axons (Ax). Also note the rhabdomere cavity (Rc) which houses the photoreceptor rhabdomeres. (G) At a higher magnification, the FM displays unique membrane invasions and spikes and is thought to support the retinal floor which faces the lamina proper. (H) The basal region of the CC processes and CC feet (ccf) in close proximity of the FM. Note the thin CC processes approaching the FM. (I) Higher magnification of the region between black arrowheads in H shows the presence of SJs (I, black arrowheads). (J, K) Below the FM, there is a layer of glial cells, the subretinal glial cells (SRG) which form extensive SJs (black arrowheads, K) at the base of the retina. Scale bars: B, 5μm; C, F, 1μm; D, G, H, 0.5μm; E, J, 0.2μm; I, K, 0.1μm.

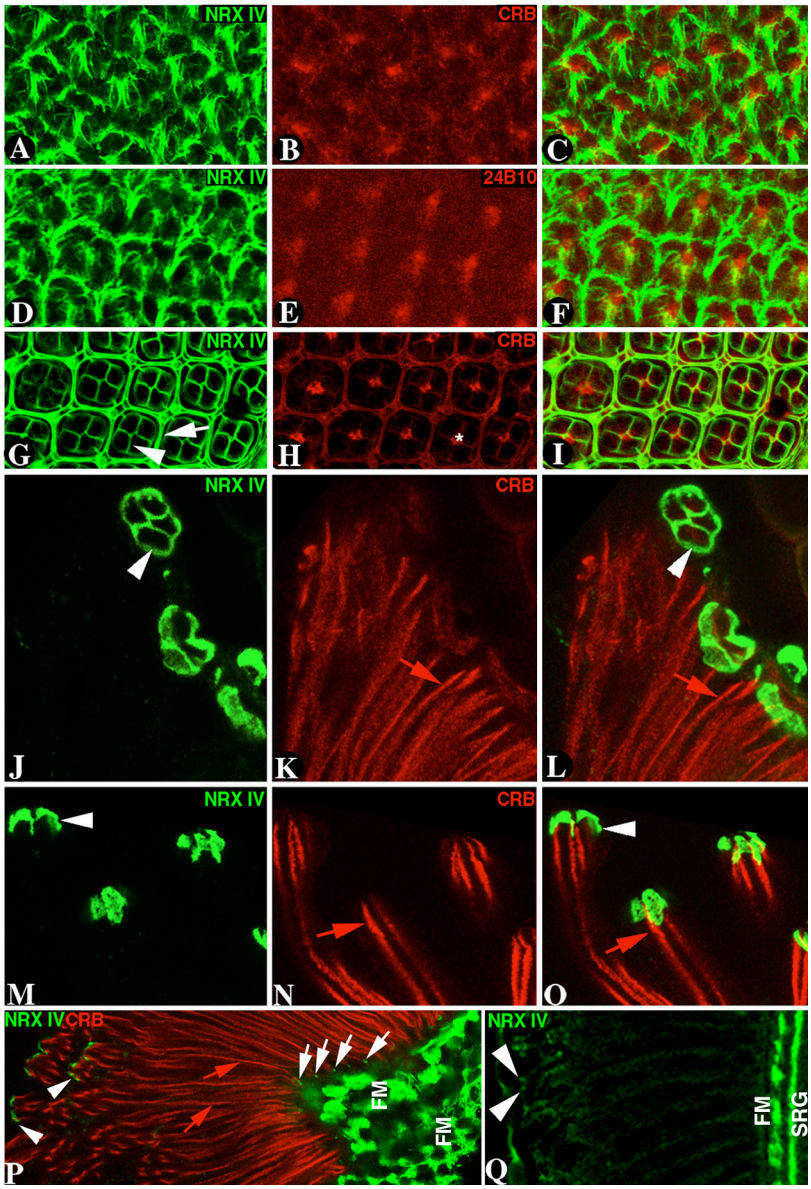

Figure 3. Nrx IV expression coincides with the presence of SJs

(A–C) Immunofluorescence localization of Nrx IV (A) and Crb (B) in the third-instar eye imaginal epithelia. Nrx IV (A, green) localizes strongly in cells posterior to the morphogenetic furrow (not shown) where as Crb (B, red) expression is on the apical surface of the cells as is evident from the merged image (C). Immunofluorescence localization of Nrx IV (D) and chaoptin (24B10) (E) in the third-instar eye imaginal epithelia. Nrx IV (D, green) localizes strongly in the disc epithelial cells and its localization is distinct from that of chaoptin (E) which localizes to the differentiating PRs. Note that Nrx IV and chaoptin localizations do not overlap as seen in the merged image (F). (G–I) A confocal image of a 37% pupal eye showing the localization of Nrx IV (G, green) and Crb (H, red). Nrx IV localizes to the CCs (white arrowhead) and PCs (white arrow). Crb localizes to the apical region of the differentiated PRs (asterisks, H and see the merged image I). (J–L) A tangential section through the adult eye shows Nrx IV (J, green) localization in the four CCs and the primary PCs, while Crb (K, red) localizes to the rhabdomere stalks only. A merged image of Nrx IV and Crb is shown in (L). (M–O) Adult ommatidia in a longitudinal view stained with Nrx IV (M, green) and Crb (N,

red) show intense localization of Nrx IV in the CC and PCs (M, O). Crb (N, O) is localized below the CCs in the apical region of the PRs and along the rhabdomere stalk. Note that Nrx IV staining forms a cap at the top of the rhabdomere stalks. (P) A confocal image showing the entire longitudinal view of the ommatidia. Note the Nrx IV immunoreactivity in the apical (white arrowhead) and basal (white arrow) regions of the ommatidia. The basal staining of Nrx IV localizes to CC feet (white arrow) and the fenestrated membrane (FM). (Q) A confocal image of a frozen section of an adult eye shows Nrx IV localization in the apical region (white arrowheads) and in the basal region where the CC feet and the fenestrated membranes (FM). Below the FM, there is staining in the subretinal glial layer (SRG).

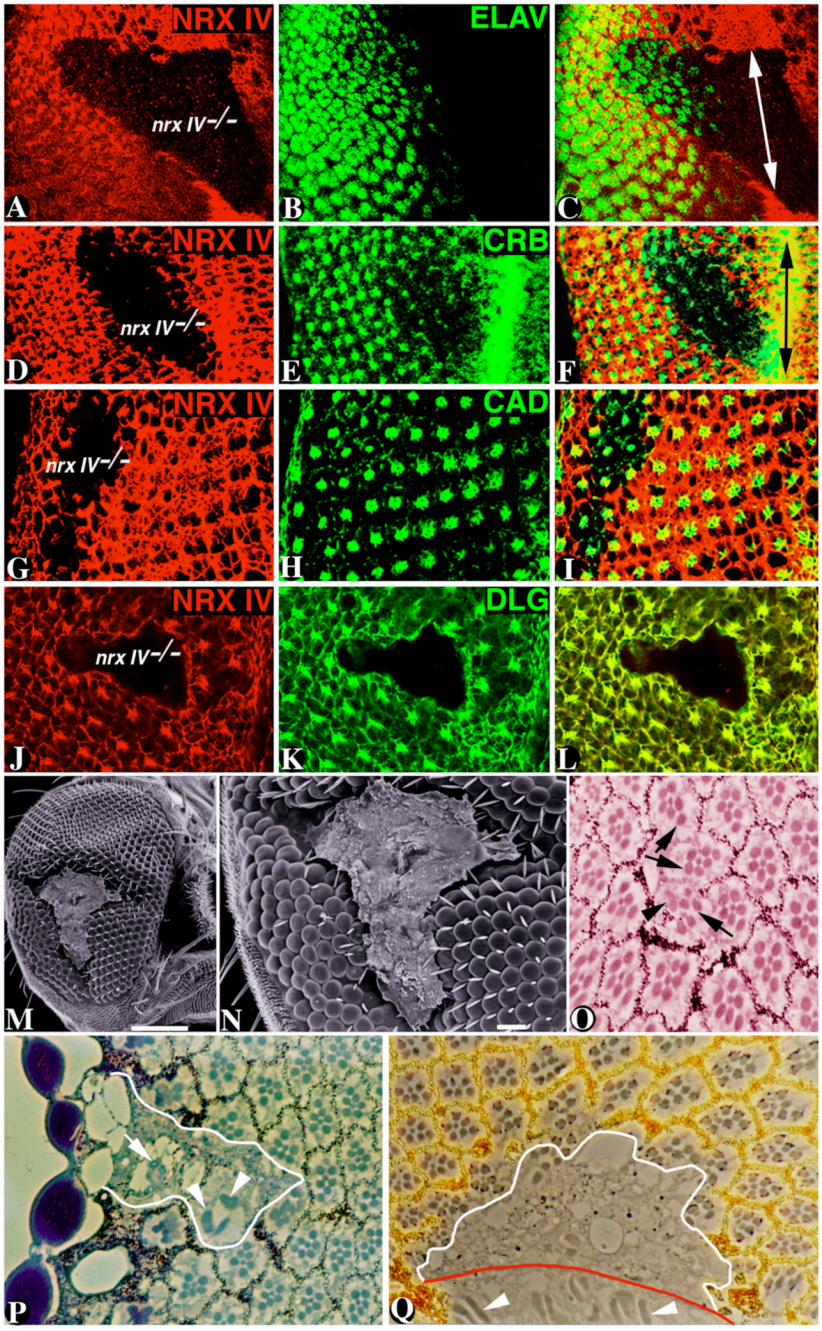

Figure 4. Clonal loss of *nrx IV* causes ommatidial collapse

(A–C) A confocal section of a third instar eye imaginal disc stained with anti-Nrx IV (A, red) and anti-Elav (B, green). *nrx IV* clones were identified based on the loss of Nrx IV immunoreactivity. Anti-Elav (B) staining revealed that PR determination is mostly normal in *nrx IV* clones (C). The double-ended arrow indicates the location of the morphogenetic furrow. The Nrx IV staining is out of focus as the focus is on the ELAV staining which is more basal than Nrx IV. (D–F) A confocal section of a third instar eye imaginal disc stained with anti-Nrx IV (D, red) and anti-Crb (E, green). Crb is present in *nrx IV* clones and localizes apically (F). (G–I) A confocal section of a third instar eye imaginal disc stained with anti-Nrx IV (G, red) and anti-cadherin (Cad, I, green). Cad (I), an AJ marker, labels PR cells at their apical portion

where they are in contact with each other. Inside the center of the clone (H and I), Cad protein is present at proper level in the cells, but the overall morphology of the various PRs looks altered in this focal plane. (J–L) A confocal section of a third instar eye imaginal disc stained with anti-Nrx IV (J, red) and anti-discs large (Dlg, K, green) shows a complete loss of the SJ protein, Dlg (K) in the *nrx IV* clones (see merge in L). At a lower focal plane, the tissue is observed with no Dlg immunoreactivity. (M) Scanning electron micrograph at a lower magnification of an adult eye with a *nrx IV* clone. Note the complete loss of ommatidia within the clone. (N) The mutant eye clone in M at a higher magnification shows a scar-like tissue. (O) A light microscopic section at the level of the *nrx IV* mutant clone based on the loss of pigment granules (w^-) shows presence of rhabdomeres (black arrows) although some rhabdomeres show structural abnormalities (black arrowhead). (P) A medium sized clone affecting several ommatidia (clone area marked by white line). The PRs in the middle of the clone are severely affected and show either loss of rhabdomeres (white arrow) or fused rhabdomeres (white arrowhead). (Q) An unstained section through a large *nrx IV* clone (clone area marked by white line). Wild-type PRs have a dot of w^+ pigment, whereas *nrx IV* mutant cells lack this pigment, allowing a cell by cell marking of the clone. Entire ommatidia and PRs are lacking inside the clone. Many aberrant rhabdomeres can be noticed beneath the retina, in the first optic station or lamina (white arrowheads). The red line indicates the retinal floor separating the retina from the lamina. Orientation: Posterior is left in A–L.

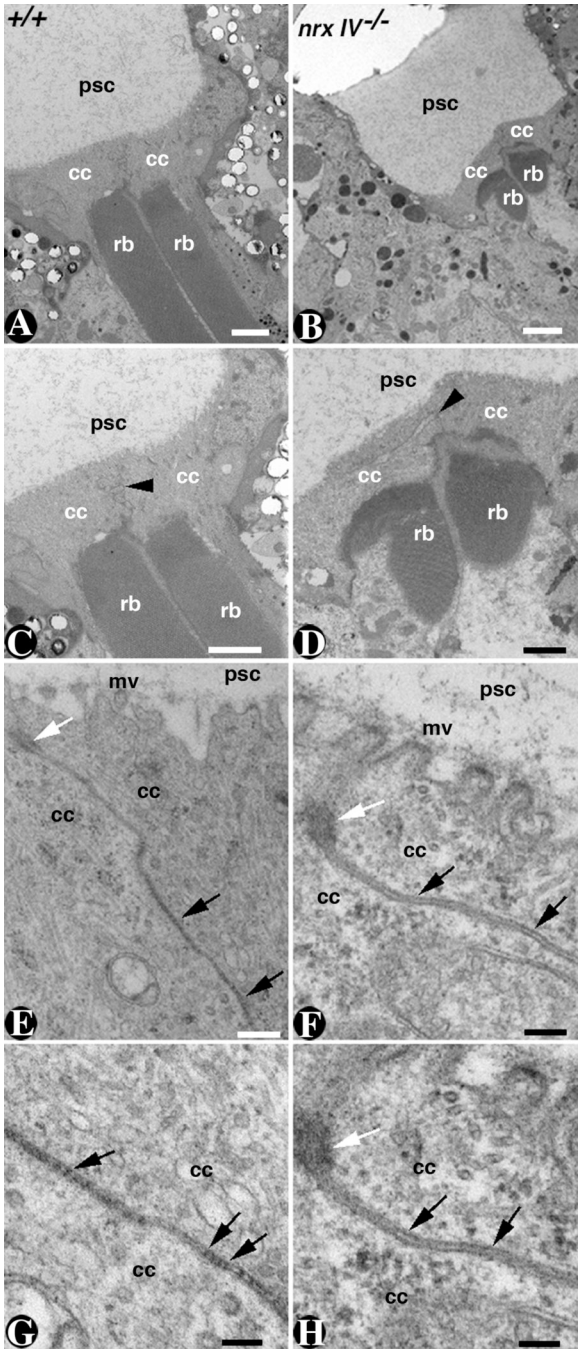

Figure 5. Cone Cell SJs are Absent in *nrx IV* Somatic Clones

(A) Electron micrograph of a longitudinal section of a wild type adult ommatidium with two CCs (cc) situated above the photorecptor rhabdomeres (rb) which stretch longitudinally. The apical regions of the CCs face the pseudocone cavity (psc). Note the pigment granules surrounding the CCs. (B) Electron micrograph of a longitudinal section of an ommatidium mutant for *nrx IV*. The CCs (cc) are present and face the pseudocone cavity (psc) and are situated above the stunted rhabdomeres (rb). Note that the pigment granules are absent from the surrounding PCs. (C, D) Higher magnification of the sections shown in (A) and (B), respectively, show regions where CC membranes establish SJs (black arrowheads, C, D). (E–H) Higher magnification TEM sections focused on the CC membranes show AJs (white arrow)

close to the apical microvilli (mv, E) and long stretches of ladder-like SJs (black arrows, E, G) in the wild type ommatidia. The CC AJs show normal electron density and morphology in *nrx IV* mutant clones as seen in the wild type (white arrows, F, H) but a complete loss of the ladder-like SJs (black arrows, F, H). Note that the intermembrane spacing has not changed between the wild type (E, G) and the *nrx IV* mutant CCs. Scale bars: A, B, 1μm; C, D, 0.5μm; E, F, 0.25μm; G, H, 0.1μm.

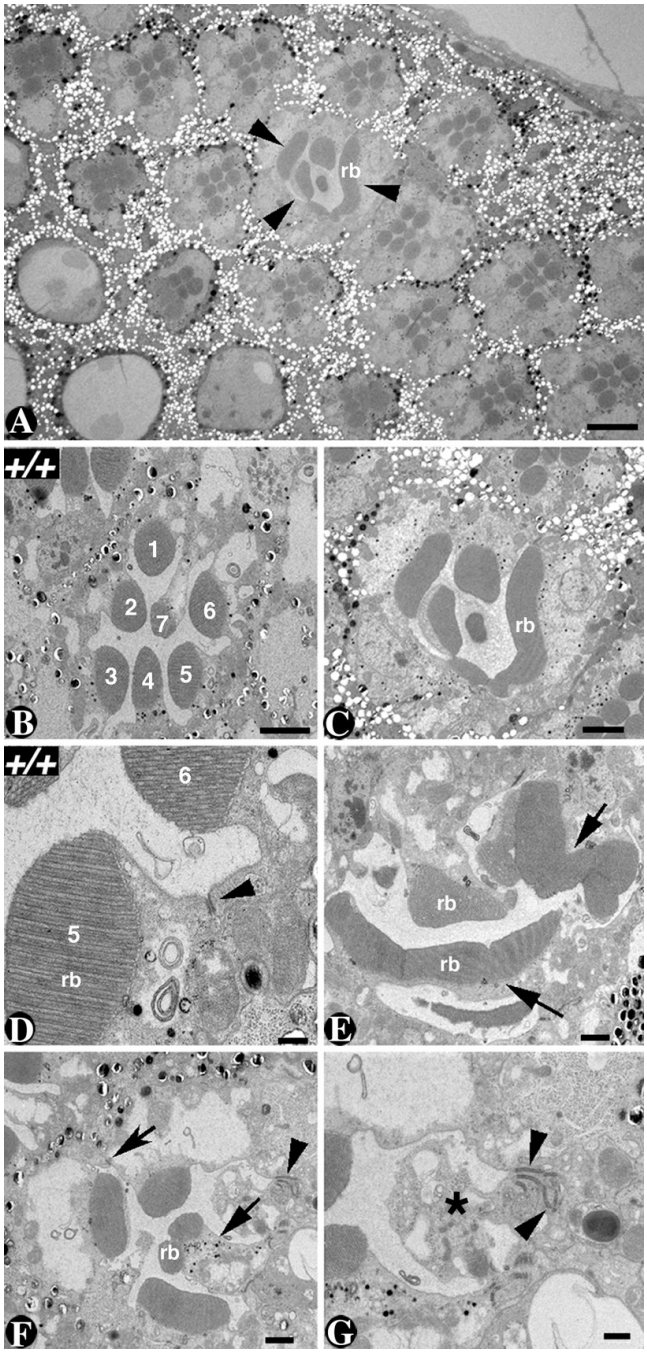

Figure 6. *nrx IV* Mutant Ommatidia Undergo Photoreceptor Degeneration

(A) An EM cross section through a *nrx IV* mutant ommatidium surrounded by the wild type ommatidia. Note the lack of pigment granules and fused rhabdomeres (rb, black arrowheads) that define the muatnt clone. (B) A wild type ommatidium showing the typical trapezoid arrangement of PR rhabdomeres (rb) facing the lumen. (C) Higher magnification of the mutant ommatidium from panel A. Note that the PR rhbdomeres (rb) are fused and have lost the typical trapezoidal arrangement seen in the wild type (B). (D) Higher magnification of two wild type photorecptor rhabdomeres (rb) joined at the stalks. Note the AJs (black arrowhead) between the stalks. (E) A *nrx IV* mutant ommatidium displaying fused, disorganized and abnormally shaped PR rhabdomeres (rb, black arrows). (F, G) A *nrx IV* mutant ommatidium with fused

photorecptor stalks and fewer rhabdomeres (rb, black arrow). The asterisk points to a degenerated PR (G) and the black arrowheads point to stretches of AJs at the base of the degenerated photorecptors (F, higher magnification in G). Scale bars: A, 5μm; B, 2μm; C, 2.5μm; D, 0.25μm; E, F, 1μm; G, 0.5μm.

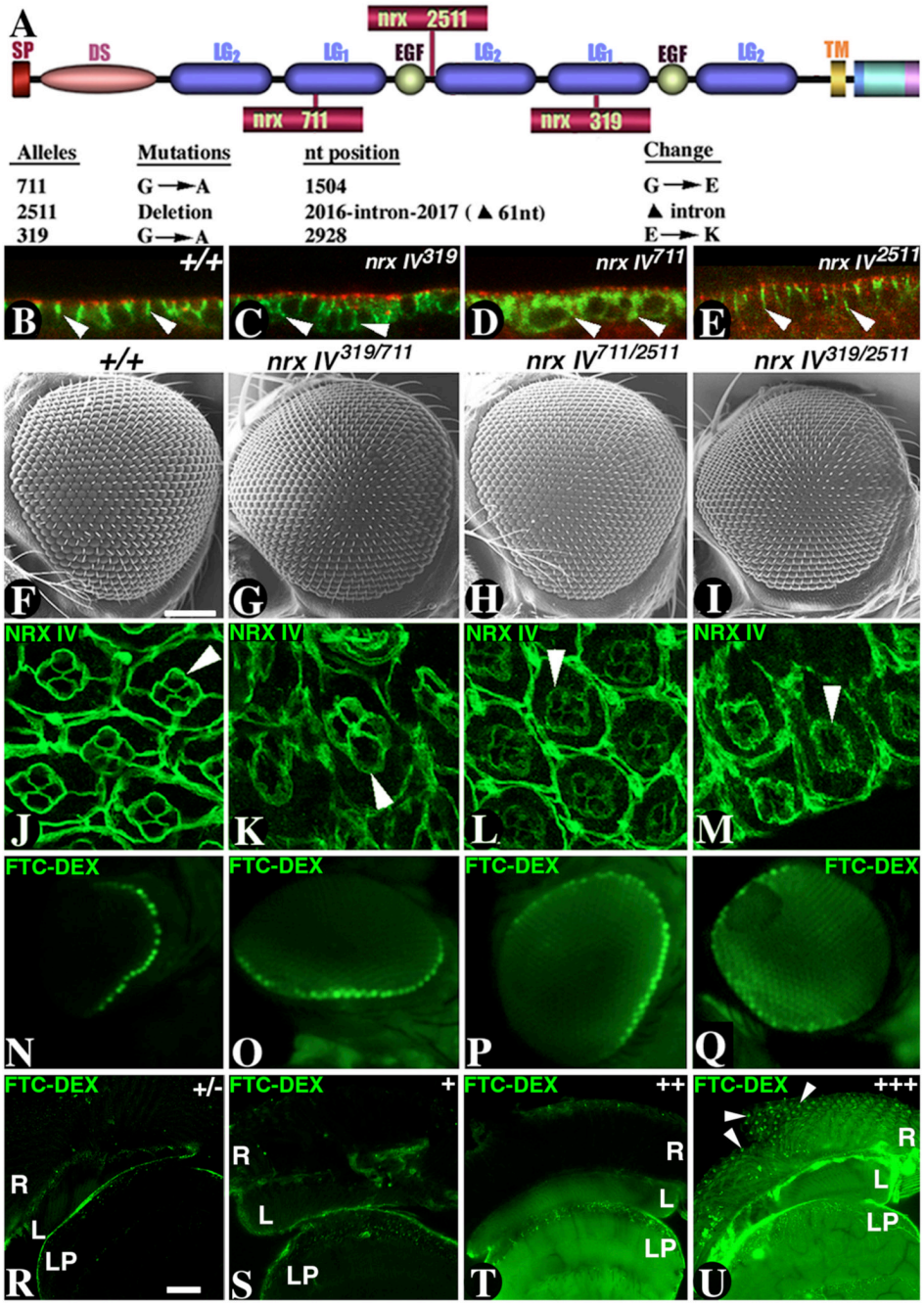

Figure 7. Blood-Eye Barrier is compromised in *nrx IV* hypomorphic mutants

(A) A cartoon depicting the domain structure of Nrx IV and molecular defects associated with three independent *nrx IV* alleles. The point mutations in *nrx IV*^{711} and *nrx IV*^{319} alleles lead to amino acid changes in the laminin G domains. *nrx IV*^{2511} has a deletion in an intron and produces reduced levels of the Nrx IV protein. (B–E) Confocal sections of stage 16 embryonic epithelia from wild type (B), *nrx IV*^{319} (C), *nrx IV*^{711} (D) and *nrx IV*^{2511} (E) immunostained against Nrx IV (green) and Crb (red). Nrx IV immunoreactivity in *nrx IV*^{319} and *nrx IV*^{711} is diffuse and fails to localize properly at SJs (compare C and D with B). In *nrx IV*^{2511}, Nrx IV levels are very low and show more basolateral distribution. Crb is normally localized in all three mutants as in the wild type. (F–I) SEM of adult eye from wild type (F) and hypomorphic

mutant combinations *nrx IV*$^{319/711}$ (G), *nrx IV*$^{711/2511}$ (H) and *nrx IV*$^{319/2511}$ (I) shows normal external eye morphology and ommatidial lattice. (J–M) Confocal sections of ommatidia from wild type (J), *nrx IV*$^{319/711}$ (K), *nrx IV*$^{711/2511}$ (L) and *nrx IV*$^{319/2511}$ (M) immunostained against Nrx IV (green). Nrx IV immunoreactivity in *nrx IV*$^{319/711}$, *nrx IV*$^{711/2511}$, and *nrx IV*$^{319/2511}$ shows a diffuse distribution in CCs and PCs. *nrx IV*$^{319/2511}$ shows the most severe phenotype with clear disruption of the CC structure (white arrowheads, compare K, L, M with J). (N–Q) The fluorescent dye FITC-dextran is excluded from the retina of control w^{-} flies (N) but penetrates in the eyes of *nrx IV* hypomorphic transheterozygous flies *nrx IV*$^{319/711}$ (O), *nrx IV*$^{711/2511}$ (P) and *nrx IV*$^{319/2511}$ (Q). Note that the dye accumulation is stronger in *nrx IV*$^{319/2511}$ eyes in panel Q compared to panels O and P reflecting a more severe phenotype and breach of the BEB. The severity of this phenotype is also reflected by Nrx IV localization in *nrx IV*$^{319/2511}$ shown in (M). (R–U) High contrast images of the cuticle bare adult fly cornea from whole live animals (*for details refer methods*). All images are taken under the same conditions maximizing contrast in a w^{-} control line. Relative leakiness of *nrx IV* hypomorphic allelic combinations was determined by comparison to control animals and representative images are shown demonstrating increasing penetration of dye into increasingly severe *nrx IV* hypomorphs. Estimates of fluorescent dye penetration were performed on multiple brains controlling for anatomic location and depth of the confocal images (N=6–15 brains depending on the quality and preparation of the tissues). WT fluorescence was set at 3–7 units and given a (+/−) value to define a limit in the background fluorescence. Based on these estimations the hypomorphic combinations were scored at *nrx IV*$^{319/711}$ (+; 12–18 units; S), *nrx IV*$^{2511/711}$ (++; 30–40 units; T) and *nrx IV*$^{319/2511}$ (+++; 60–90 units; U).

Genotypes: F, J, N, R (+/+); G, K, O, S (*nrx IV*$^{319/711}$); H, L, P, T (*nrx IV*$^{2511/711}$) and I, M, Q, U (*nrx IV*$^{319/2511}$)

Abbreviations: R=retina, L=lamina, Lp=lobular plate. Scale bar: F–I, 100μm; R–U, 10μm.

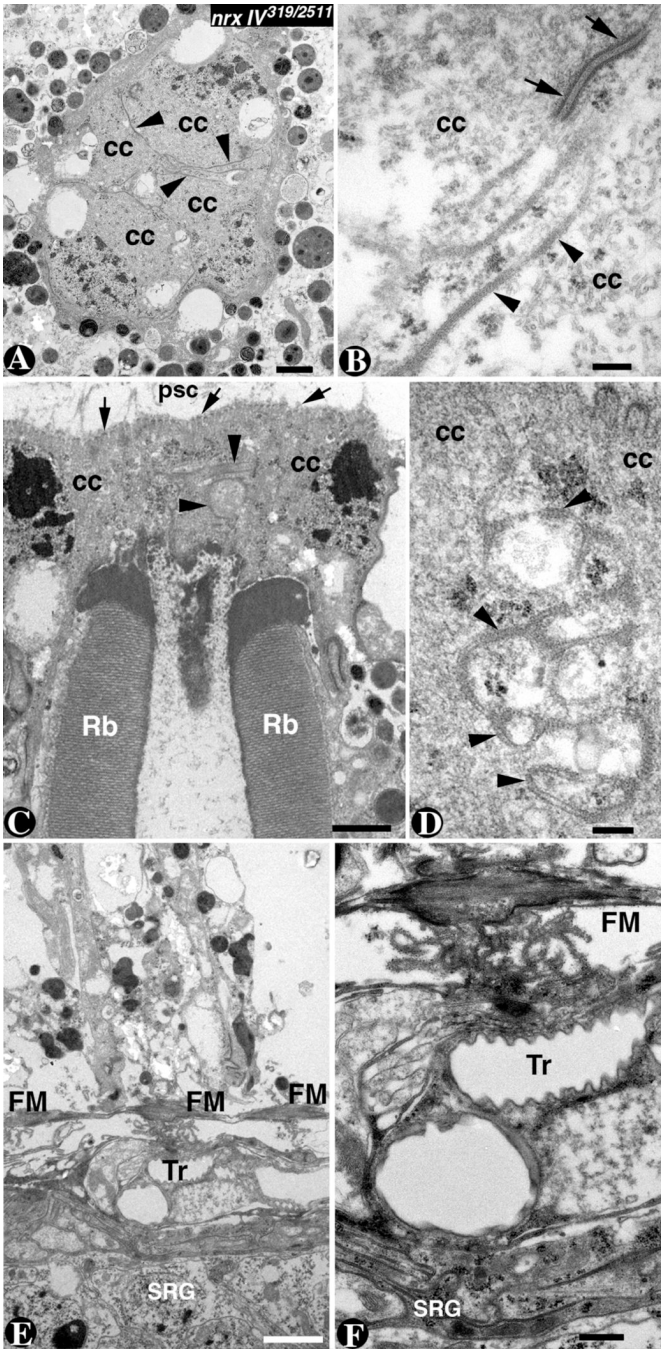

Fig. 8. Ultrastructural SJ morphology is Affected in *nrx IV* Hypomorphic Alleles

(A) TEM section showing the 4 CC arrangement in *nrx IV*$^{319/2511}$ mutants. The electron densities at the CC interface at this magnification (black arrowheads) is similar to that seen in the wild type (refer Fig. 1G). (B) At a higher magnification the CC SJs display an abnormal morphology (black arrowheads) where as the morphology of AJs is unaffected (black arrows). (C) A longitudinal section through the mutant ommatidium shows normal cellular organization as seen by the arrangement of the CCs and PR rhabdomeres (Rb). The SJ areas (black arrowheads) are also visible. (D) A higher magnification of the SJ areas in C reveals defective SJs with unstructured and fuzzy electron densities. Note that the intermembrane distance is maintained at about 17–20nm. (E, F) The basal regions of the ommatidia show normal

organization of the retinal floor with well-formed fenestrated membrane (FM) and the glial layer below, the subretinal glia (SRG).